



# Fermi National Accelerator Laboratory

FERMILAB-Pub-83/99-EXP  
7550.580  
(Submitted to Phys. Rev.)

DIFFRACTIVE PRODUCTION OF  $K_S^0 K_S^0 \pi^+ \pi^- \pi^-$  IN  $\pi^- N$  INTERACTIONS AT 200 GeV/c

C. C. Chang, T. C. Davis, R. N. Diamond, K. J. Johnson,  
R. W. Joyner, and J. A. Poirier  
University of Notre Dame, Notre Dame, Indiana 46556

T. Y. Chen, E. W. Jenkins, K. W. Lai, J. LeBritton,  
Y. C. Lin, and A. E. Pifer  
University of Arizona, Tucson, Arizona 85721

H. C. Fenker and D. R. Green  
Fermi National Accelerator Laboratory, Batavia, Illinois 60510

J. R. Albright, J. H. Goldman, S. L. Hagopian, J. E. Lannutti, and J. E. Piper  
Florida State University, Tallahassee, Florida 32306

A. Napier  
Tufts University, Medford, Massachusetts 02155

J. M. Marraffino, J. W. Waters, M. S. Webster, and E. G. H. Williams  
Vanderbilt University, Nashville, Tennessee 37235

and

J. R. Ficencic and W. P. Trower  
Virginia Polytechnic Institute and State University  
Blacksburg, Virginia 24061

November 1983



Diffractive Production of  $K_S^0 K_S^0 \pi^+ \pi^- \pi^-$  in  $\pi^- N$  Interactions  
at 200 GeV/c

C.C. Chang, T.C. Davis, R.N. Diamond<sup>a</sup>, K.J. Johnson<sup>b</sup>,  
R.W. Joyner, and J.A. Poirier  
University of Notre Dame, Notre Dame, Indiana 46556

T.Y. Chen<sup>c</sup>, E.W. Jenkins, K.W. Lai, J. LeBritton<sup>d</sup>,  
Y.C. Lin<sup>e</sup>, and A.E. Pifer  
University of Arizona, Tucson, Arizona 85721

H.C. Fenker and D.R. Green  
Fermilab, Batavia, Illinois 60510

J.R. Albright, J.H. Goldman, S.L. Hagopian,  
J.E. Lannutti, and J.E. Piper  
Florida State University, Tallahassee, Florida 32306

A. Napier  
Tufts University, Medford, Massachusetts 02155

J.M. Marraffino, J.W. Waters, M.S. Webster, and E.G.H. Williams  
Vanderbilt University, Nashville, Tennessee 37235

J.R. Ficenec, and W.P. Trower  
Virginia Polytechnic Institute and State University,  
Blacksburg, Virginia 24061

November 1, 1983

ABSTRACT

The diffractive dissociation of a 200 GeV/c  $\pi^-$  beam into  $K_S^0 K_S^0 \pi^+ \pi^- \pi^-$  has been observed. The diffractive  $K_S^0 K_S^0 \pi^+ \pi^- \pi^-$  cross section is  $1.59 \pm 0.78$   $\mu\text{b}$ . The ratio of the diffractive  $K_S^0 K_S^0 \pi^+ \pi^- \pi^-$  cross section to the diffractive  $K_S^0 K_S^0 \pi^-$  cross section is  $0.40 \pm 0.13$  which is in good agreement with a diffractive fragmentation model prediction of 0.36. There is evidence for simultaneous production of  $K^{*-}$  and  $K^{*+}$  in the diffractive  $K_S^0 K_S^0 \pi^+ \pi^- \pi^-$  sample. The  $K^{*+} - K_S^0 \pi^-$  mass distribution shows an enhancement near 1.95 GeV.

Although diffractive dissociation has been widely observed in high energy hadroproduction experiments<sup>1,2,3</sup>, relatively little information is available on the flavor dependence of this process. We present here the latest, highest energy results on the diffractive dissociation of a 200 GeV/c  $\pi^-$  beam into  $K_S^0 K_S^0 \pi^+ \pi^- \pi^-$ .

In the diffractive fragmentation model<sup>4</sup> the secondary particles are considered to be fragments of either the beam particle or the target particle and can be divided into: a) forward particles coming from the fragmentation of the beam particle; and b) backward particles coming from the fragmentation of the target particle. This tendency to go separately into the forward and backward hemispheres in the center-of-mass system increases with increasing beam energy.

Our experiment was designed to detect the forward outgoing particles from a high energy (200 GeV/c)  $\pi^-$  beam. The experiment triggered on events with two neutral strange particles accompanied by a limited number,  $n$  ( $\leq 5$ ), of charged primaries. Good acceptance in mass and momentum transfer was achieved with a large aperture superconducting dipole spectrometer magnet. This provided a unique opportunity to study the diffractive fragmentation of a  $\pi^-$  beam into  $K_S^0 K_S^0 (n\pi)^-$ . The  $K_S^0 K_S^0 \pi^-$  system has been reported previously<sup>5</sup>.

In this paper we present results for the diffractive process

$$\pi^- N \rightarrow K_S^0 K_S^0 \pi^+ \pi^- \pi^- N'.$$

The data for this analysis are derived from experiment E580 using the Multiparticle Spectrometer at Fermi National Accelerator Laboratory. Details of the experiment and our method of selecting  $K_S^0 K_S^0 (n\pi)^-$  events have been given previously<sup>5</sup>. A  $K_S^0 K_S^0 \pi^+ \pi^- \pi^-$  sample of 2767 events was obtained by requiring the total visible energy  $< 220$  GeV and the distance of closest approach of each track to the primary vertex to be less than four  $\sigma$ .

For the present study we make one additional cut:  $X_F > 0$  (for each outgoing particle), where  $X_F = 2P_L^{CM} / \sqrt{s}$ . This cut serves to separate the beam from the target fragmentation region. After this cut there remains a sample of 2734  $K_S^0 K_S^0$  events with one positive primary track and two negative primary tracks passing through the spectrometer. The sum of the  $\Lambda$  and  $\bar{\Lambda}$  contaminations in this sample is estimated to be 2%. To isolate the diffractive component in our  $K_S^0 K_S^0 \pi^+ \pi^- \pi^-$  data, we plot the recoiling mass squared ( $MM^2$ ) as the unshaded histogram of Fig. 1(a), assuming a nucleon target. The low mass peak centered at  $1 \text{ GeV}^2$  is interpreted as the recoiling nucleon system. We will take as our diffractive sample for subsequent calculations the 392 events with  $MM^2 < 16 \text{ GeV}^2$ .

The geometrical acceptance was calculated for these diffractive events by producing for each observed event 100

identical events rotated about the beam axis. Each particle was traced through the aperture of the magnet and tracking chambers while avoiding a beam veto counter. The mean geometrical efficiency for events with  $MM^2$  less than  $16 \text{ GeV}^2$  is 87.4%. This acceptance is reduced to 18.5% when both  $K_S^0$ 's are required to decay within the 2.14 m long decay volume beginning 0.73 m downstream from the center of the target.

In the analysis of exclusive reactions considerable effort is made to eliminate or correct for the non-diffractive background. The shaded histogram in Fig. 1(a) shows the recoiling mass squared distribution of the  $K_S^0 K_S^0 \pi^+ \pi^+ \pi^-$  system. As expected, we do not see the low mass peak in this figure since the net + charge of this final state could not be produced diffractively. Since this final state of two neutral  $K_S^0$ 's and three  $\pi$ 's has the same number of particles as the  $K_S^0 K_S^0 \pi^+ \pi^- \pi^-$  state we use this data as an estimate of the non-diffractive background in the  $K_S^0 K_S^0 \pi^+ \pi^- \pi^-$  channel. Smoothing this shaded histogram and normalizing it to the unshaded histogram of Fig. 1(a) between  $80 \text{ GeV}^2$  and  $200 \text{ GeV}^2$ , we obtain the solid curve shown in the figure; subtracting, we obtain Fig. 1(b).

In Fig. 1(b) we observe a second peak near  $22 \text{ GeV}^2$  and postulate that this peak comes from diffractive events with an unseen  $\pi^0$ . In order to investigate this second peak we assume that the effect on the  $MM^2$  distribution caused by removing a  $\pi^0$

from  $K_S^0 K_S^0 \pi^+ \pi^- \pi^- \pi^0$  is similar to removing the  $\pi^+$  from  $K_S^0 K_S^0 \pi^+ \pi^- \pi^-$ . We therefore use the  $K_S^0 K_S^0 \pi^+ \pi^- \pi^-$  events with  $MM^2 < 16 \text{ GeV}^2$ , throw out the only  $\pi^+$ , recalculate the missing mass squared of the remaining  $K_S^0 K_S^0 \pi^- \pi^-$  and plot it in Fig. 1(c). A mass peak near  $22 \text{ GeV}^2$  is obtained, and thus it can be inferred that  $K_S^0 K_S^0 \pi^+ \pi^- \pi^- \pi^0$  diffractive events are in our  $K_S^0 K_S^0 \pi^+ \pi^- \pi^-$  sample. In support of this idea we also looked at the missing mass squared of  $K_S^0 K_S^0 \pi^- \pi^-$  from  $K_S^0 K_S^0 \pi^- \pi^-$  events and observed a similar enhancement around  $22 \text{ GeV}^2$ , presumably from a missing  $\pi^+$ .

We now determine the number of  $K_S^0 K_S^0 \pi^+ \pi^- \pi^-$  diffractive events and then determine the cross section. Normalizing the histogram in Fig. 1(c) between  $20 \text{ GeV}^2$  and  $200 \text{ GeV}^2$  to the histogram in Fig. 1(b) and then subtracting, we obtain the result shown in Fig. 1(d). A prominent low mass peak results whose FWHM is consistent with the calculated spectrometer  $MM^2$  resolution of  $11.2 \text{ GeV}^2$  (FWHM). In this figure there are 249 events with  $MM^2 < 16 \text{ GeV}^2$  which are assumed to be primarily single diffractive events plus some double diffractive events and 119 events with  $16.0 \text{ GeV}^2 < MM^2 < 60 \text{ GeV}^2$  which are predominantly double diffractive events. The double diffraction, which has a  $1/MM^2$  behavior<sup>6</sup>, is estimated to be  $\sim 1/3$  of the total  $MM^2$  signal<sup>7</sup>. We take our cut at  $MM^2 < 16 \text{ GeV}^2$  to minimize the background from inelastic non-diffractive processes amounting to  $26 \pm 3\%$ , while double diffraction is  $1.1 \pm 0.5\%$  and  $K_S^0 K_S^0 \pi^+ \pi^- \pi^- \pi^0$  is  $10.8 \pm 1.7\%$  of the 392 surviving events. Removing

these backgrounds,  $245 \pm 24$   $K_S^0 K_S^0 \pi^+ \pi^- \pi^-$  single diffractive events remain. To check our result, we use the same method as in our  $K_S^0 K_S^0 \pi^-$  diffractive paper<sup>5</sup> to fit the  $MM^2$  distribution for  $K_S^0 K_S^0 \pi^+ \pi^- \pi^-$  events, and  $230 \pm 15$   $K_S^0 K_S^0 \pi^+ \pi^- \pi^-$  single diffractive events are obtained. Comparing the geometrical acceptances and decay efficiencies for  $K_S^0 K_S^0 \pi^+ \pi^- \pi^-$  events and  $K_S^0 K_S^0 \pi^-$  events<sup>5</sup> we obtain a sensitivity of  $240 \pm 80$  events/ $\mu\text{b}$ . The cross section for single diffractive  $K_S^0 K_S^0 \pi^+ \pi^- \pi^-$ , after correcting for the unseen decay modes of the  $K_S^0$ , is then  $1.59 \pm 0.78$   $\mu\text{b}$ . The ratio of the diffractive  $K_S^0 K_S^0 \pi^+ \pi^- \pi^-$  cross section to the diffractive  $K_S^0 K_S^0 \pi^-$  cross section is  $0.40 \pm 0.13$ , in good agreement with the value 0.36 expected in the diffractive fragmentation picture<sup>4</sup> assuming for the asymptotic topological cross sections  $\sigma = C/NTOT^2$ , where  $C$  is a constant and  $NTOT$  is the multiplicity for charged plus neutral particles.

In Fig. 2, we plot the variable  $t'$ , where  $t' = t_{\min} - t$ ,  $t$  is the square of the four-momentum transfer from the beam to the  $K_S^0 K_S^0 \pi^+ \pi^- \pi^-$  system, and  $t_{\min}$  is the minimum momentum transfer allowed kinematically. The slope of the  $dN/dt'$  distribution at large  $t'$  values is about that for elastic scattering on a single nucleon, while the slope for small  $t'$  values is about that expected for coherent elastic scattering on the entire carbon nucleus. Since our scintillator target contains 50% protons and 50% carbon nuclei, we would expect two different slopes for small  $t'$  values, one for coherent carbon target events and another for single nucleon target events. Our  $t'$  resolution ( $\sigma \sim 0.043$   $\text{GeV}^2$  at low  $t'$ ) is such that coherent production from the

carbon nuclei in our target would appear when  $t' < 0.04 \text{ GeV}^2$ , while production from protons and neutrons in our target would appear at higher  $t'$  values.

Fitting Fig. 2 by the sum of three exponentials,

$$dN/dt' = A_1 B_1 \exp(-B_1 t') + A_2 B_2 \exp(-B_2 t') + A_3 B_3 \exp(-B_3 t')$$

yields  $A_1 = 78.5 \pm 9.4$ ,  $A_2 = 167 \pm 16$ , and  $A_3 = 147 \pm 18$  events for the amplitudes and  $B_1 = 69.0^{+8.4}_{-16.4}$ ,  $B_2 = 5.4^{+0.8}_{-0.6}$ , and  $B_3 = 1.16 \text{ GeV}^{-2}$  (fixed) for the slopes. The value of the slope parameter  $B_3$  is obtained in fitting the  $t'$  distribution for events with  $MM^2 < 16 \text{ GeV}^2$ . The value of slope parameter  $B_1$  is consistent with the values found in other carbon target experiments<sup>8,9</sup>. This coherent carbon effect was not seen in the previous  $K_S^0 K_S^0 \pi^-$  diffractive sample because of a trigger bias<sup>5</sup>; this trigger bias is not operative here due to the additional charges in the final state. The slope parameter  $B_2$  in this  $KK3\pi$  sample is smaller than the value  $9.6 \pm 1.9$  obtained in the  $KK\pi^-$  data from this experiment<sup>5</sup>. This difference is in qualitative agreement with other experiments which show a decrease in slope with increasing final state mass<sup>10</sup>.

We now discuss the mass spectrum of the diffractive signal. The  $K_S^0 K_S^0$  mass distribution is shown in Fig. 3(a). Peaks are visible in the regions of the  $S^*$ ,  $f/A_2$ , and possibly the  $f'$  mesons. The  $S^*$  is more prominent in the  $X_F < 0.25$  region while

$f/A_2$  and  $f'$  are more prominent in the  $X_F > 0.5$  region as shown in Figs. 3(b) and 3(c) respectively.

The mass distribution of  $K_S^0 \pi^-$  combinations is shown in Fig. 4(a) with four entries per event. A very prominent  $K^{*-}(890)$  signal is seen, and some enhancement in the  $K^{*-}(1430)$  region is seen. We determine the resonance production cross sections by fitting the  $K_S^0 \pi^-$  mass spectrum using an incoherent sum of two Breit-Wigner resonance (BW) terms: (one for  $K^{*-}(890)$ ,  $F_{BW1}$ , and the other for  $K^{*-}(1430)$ ,  $F_{BW2}$ ); and a background (BG) term,

$$d\sigma/dm = F_{BG}(m) \left[ 1.0 + a_1 F_{BW1}(m) + a_2 F_{BW2}(m) \right] \quad (1)$$

where the  $a_1$  and  $a_2$  are parameters to be determined.

The Breit-Wigner function we use is

$$F_{BW}(m) = \frac{m m_R \Gamma(m)}{(m^2 - m_R^2)^2 + m_R^2 \Gamma^2(m)} \quad (2)$$

with

$$\Gamma(m) = \Gamma_R (q/q_R)^{2\ell+1} \rho(m) / \rho(m_R) \quad (3)$$

and

$$\rho(m) = (q_R^2 + q^2)^{-1} \quad (4)$$

In the above expressions,  $m_R$  is the resonance mass,  $\Gamma_R$  is its width,  $q$  is the momentum of one of the decay products in the resonance rest frame,  $q_R$  is the  $q$  value at  $m = m_R$ , and  $l$  is the relative angular momentum. The mass and width are held to their nominal values<sup>11</sup>. To describe the background, we use the formula

$$F_{BG}(m) = a_3 (m - m_t)^c \exp(-dm - em^2) \quad (5)$$

where  $a_3$ ,  $c$ ,  $d$ , and  $e$  are parameters and  $m_t$  is the threshold mass for  $K\pi^-$ . In Fig.4(a) the solid curve is a fit using equation (1) and the dashed curve is from equation (5). In this fit there are a total of  $130 \pm 20$   $K^{*-}(890) \rightarrow K_S^0 \pi^-$  combinations and  $45 \pm 13$   $K^{*-}(1430) \rightarrow K_S^0 \pi^-$  combinations with a  $\chi^2/NDF$  of 1.79. In order to obtain the correct number of  $K^{*-}(890)$ 's in the 245 event  $K_S^0 K_S^0 \pi^+ \pi^- \pi^-$  single diffractive sample, we do a similar fit to the  $K_S^0 \pi^-$  mass plot for 2342  $K_S^0 K_S^0 \pi^+ \pi^- \pi^-$  events with  $MM^2 > 16 \text{ GeV}^2$ , and find that there are  $398 \pm 60$   $K^{*-}(890)$ 's and  $90 \pm 18$   $K^{*-}(1430)$ 's. Assuming the same percentage of  $K^{*-}(890)$  in the background events with  $MM^2 < 16 \text{ GeV}^2$ , we subtract  $25 \pm 6$  background  $K^{*-}(890)$  events from the total and obtain  $105 \pm 21$   $K^{*-}(890)$  events corresponding to  $42 \pm 10\%$  of the single diffractive signal.

The mass distribution of the  $K_S^0 \pi^+$  combinations from  $K_S^0 K_S^0 \pi^+ \pi^- \pi^-$  events with  $MM^2$  less than  $16 \text{ GeV}^2$  is shown in Fig. 4(b). A very prominent  $K^{*+}(890)$  signal is seen, as well as a

small enhancement in the  $K^{*+}(1430)$  region. We estimate the amount of  $K^{*+}$  in the same way as above and obtain  $63 \pm 13$   $K^{*+}(890)$ 's and  $15 \pm 9$   $K^{*+}(1430)$ 's with a  $\chi^2/\text{NDF} = 1.14$ . When  $13 \pm 3$   $K^{*+}(890)$ 's not produced by single diffractive interactions are subtracted, the remaining  $50 \pm 14$   $K^{*+}(890)$ 's represent  $20 \pm 6\%$  of the single diffractive  $K_S^0 K_S^0 \pi^+ \pi^- \pi^-$  events.

Figure 5 is the  $M(K_S^0 \pi^+)$  vs.  $M(K_S^0 \pi^-)$  scatter plot with four entries per event. We note an accumulation of events in the  $K^{*+}$  and  $K^{*-}$  bands ( $0.8225 \leq M(K_S^0 \pi^{+-}) \leq 0.9575$  GeV) and an additional accumulation in the overlap region due to the double resonance final state  $K^{*+}(890)K^{*-}(890)\pi^-$ . In order to subtract the background from this overlap region we construct eight neighboring boxes; the contents of these nine boxes and the mass values of their boundaries are shown in Table I. Each of the nine regions has the same area ( $0.135 \times 0.135$  GeV<sup>2</sup>) and is separated by 0.0225 GeV from its neighbors. Figure 6 shows the  $K_S^0 K_S^0 \pi^+ \pi^-$  mass obtained from: (a) the central  $K^{*+}K^{*-}$  region, (c) the corner  $K_S^0 K_S^0 \pi^+ \pi^-$  background regions, and (b) the remaining non-diagonal  $K^{*+}K_S^0 \pi^-$  regions.

We assume that the  $K^{*+}K_S^0 \pi^-$  plus  $K_S^0 \pi^+ K^{*-}$  signal,  $K^{*B}$ , is distributed according to a single Breit-Wigner resonance shape of fixed width and mass and integrated over the appropriate limits for each region; that the  $K^{*+}K^{*-}$  signal is distributed according to the product of two Breit-Wigner forms

appropriately integrated for each region; and that the uncorrelated  $K_S^0 \pi^+ K_S^0 \pi^-$  background, BB, is distributed uniformly. In extracting the signals we are led to the matrix equation

$$\begin{pmatrix} \text{Mid} \\ \text{Non} \\ \text{Cor} \end{pmatrix} = \begin{pmatrix} 0.7773 & 0.2939 & 0.1111 \\ 0.2087 & 0.6272 & 0.4444 \\ 0.0140 & 0.0789 & 0.4444 \end{pmatrix} \begin{pmatrix} K^* K^* \\ K^* B \\ BB \end{pmatrix} \quad (6)$$

where Mid is the middle region with 84 entries, Cor is the corner regions totalling 127 entries, and Non is the remaining non-diagonal regions totalling 184 entries. The inverse matrix,  $M^{-1}$ , solves this equation and gives the result:

$$\begin{aligned} K^* K^* &= 35 \pm 17 \text{ events,} \\ K^* B &= 92 \pm 36 \text{ events, and} \\ BB &= 268 \pm 30 \text{ events} \end{aligned}$$

for the signals in the nine regions of Table I. As Table I contains only 76% of the  $K^{*+}(890)K^{*-}(890)$  signal, there are a total of  $46 \pm 22$  such events corresponding to  $12 \pm 6\%$  of the diffractive  $K_S^0 K_S^0 \pi^+ \pi^- \pi^-$  data. In order to obtain the fraction of single diffractive events with double  $K^*$  production, we subtract  $3.2 \pm 2.8$  events under the assumption that the  $2.2 \pm 1.9\%$  of events with  $MM^2 > 16 \text{ GeV}^2$  which exhibit a  $K^{*+}(890)K^{*-}(890)$  signal also represents the background in the diffractive sample. We are thereby led to

a single diffractive  $K^{*+}(890)K^{*-}(890)\pi^-$  signal of  $43 \pm 22$  events which is  $18 \pm 9\%$  of the single diffractive sample.

Figure 7(a) shows the  $K^{*+}(890)K^{*-}(890)$  mass distribution with errors obtained by combining the data from the nine regions according to the inverse matrix  $M^{-1}$ . Figure 7(b) shows the  $K^{*+}K_S^0\pi^-\pi^+$  mass distribution with errors obtained in a similar fashion; a possible enhancement is seen at a mass of 1.95 GeV. The data are plotted in 80 MeV bins because of the limited statistics; the mass resolution is typically 35 MeV.

In figure 8, we plot the  $K_S^0K_S^0\pi^+\pi^-\pi^-\pi^+$  mass for those events with  $MM^2 < 16 \text{ GeV}^2$ . The shaded histogram consists of those events which in addition have a  $K_S^0\pi^+$  and  $K_S^0\pi^-$  combination in the center box of Table I and which contains the largest  $K^{*+}(890)K^{*-}(890)$  sample. Within the limited statistics neither histogram shows significant structure.

As there is no need to restrict the  $K_S^0\pi^{+-}$  masses to the regions of Table I, we show in figure 9 the  $K_S^0K_S^0\pi^+\pi^-\pi^-\pi^+$  mass for all combinations which satisfy a  $K^*(890)$  mass cut from 0.8225 to 0.9575 GeV. A background subtraction has been performed using combinations with a  $K\pi$  mass from 0.665 to 0.800 GeV or 0.980 to 1.115 GeV. The peak at 1.95 GeV is even more prominent than in Fig. 7(b). By combining histograms 7(a) and 7(b) one would obtain a  $K^*(K\pi \text{ inclusive})$  mass distribution similar to that of

Fig. 9 but with lower statistics since the  $K_{\pi}$  masses would be restricted to the mass regions in Table I.

In summary, we observe the diffractive dissociation of  $\pi^{-}$  into  $K_S^0 K_S^0 \pi^+ \pi^- \pi^-$ . The diffractive  $K_S^0 K_S^0 \pi^+ \pi^- \pi^-$  system exhibits resonant state particles like  $K^{*+-}(890)$ ,  $f/A_2$ , and  $f'$ . The ratio of the diffractive  $K_S^0 K_S^0 \pi^+ \pi^- \pi^-$  cross section to the diffractive  $K_S^0 K_S^0 \pi^-$  cross section is  $0.40 \pm 0.13$  which is in good agreement with 0.36 expected in the diffractive fragmentation picture. Finally, we observe  $43 \pm 22$  events with correlated resonance production in the diffractive process

$$\pi^{-} N \rightarrow K^{*+}(890) K^{*-}(890) \pi^{-} N'$$

where the  $K^{*+-}(890)$  decays to  $K_S^0$  and a  $\pi^{+-}$ . We also observe an enhancement in the  $K^{*+-} K_S^0 \pi^{-+}$  system at a mass of 1.95 GeV.

We thank the Fermilab staff, especially S. Hansen and R. Cantel, for their valuable help during the experiment. Z. Ma provided helpful support. The work was supported in part by Department of Energy contracts (Arizona, Florida State, Tufts) and National Science Foundation grants (Arizona, Notre Dame, Vanderbilt and Virginia Tech.).

## Footnotes and References

(a) Former address: Florida State U., Tallahassee, Florida  
32306

(b) Present address: Motorola Inc., Phoenix, Arizona 85008

(c) Present address: Dept. of Physics, Nanking U., Nanking,  
People's Republic of China

(d) Present address: Burr-Brown Research Corp., Tucson, Arizona  
85706

(e) Present address: 1782 Calle Yucca, Thousand Oaks, California  
91360

1. R. L. Cool et al., Phys. Rev. Lett. 47, 701 (1981)  
and references therein. See also A. B. Kaidalov,  
Phys. Repts. 50, 157(1979).
2. G. Otter et al., Nucl. Phys. B96, 365(1975); R.  
Diamond et al., Phys. Rev. D7, 1977(1973).
3. C. Daum et al., Nucl. Phys. B182, 269(1981).
4. R. C. Hwa, Phys. Rev. Lett. 26, 1143 (1971).
5. T. Y. Chen et al., Diffractive Production of  $K_S^0 K_S^0 \pi^-$  in

$\pi^-$ N Interactions at 200 GeV/c, to be published in Physical Review. T. Y. Chen et al., Fermilab-Pub-82/94-EXP. For the present layout see J. Poirier et al., in Multiparticle Dynamics 1981, edited by W. D. Shephard and V. P. Kenney (World Scientific, Singapore, 1982) P. 153.

6. R. G. Roberts in Phenomonology of Particles at High Energy, edited by R. L. Crawford and R. Jennings (Academic Press, 1974) p. 201; D. P. Roy and R. G. Roberts Nucl. Phys. B77, 240(1974).
7. M. G. Albrow et al., Nucl. Phys. B108, 1(1976), J. W. Lämsä et al., Phys. Rev. D18, 3933(1978), A. Givernaud et al., Nucl. Phys. B152, 189(1979).
8. R. M. Edelstein et al., Phys. Rev. Lett. 38, 185 (1977).
9. D. D. O'Brien et al., Nucl. Phys. B77, 1(1974).
10. H. J. Lubatti and K. Moriyasu, Lett. Nuovo Cimento 13,97 (1975).
11. Particle Data Group, Phys. Lett. 111B, 1(1982).

Table I

 $K_S^0 \pi^-$  Mass (GeV)

23	45	32	1.1150	
47	84	46	0.9800	$K_S^0 \pi^+$
			0.9575	Mass
			0.8225	(GeV)
35	46	37	0.8000	
			0.6650	

Table Captions

- I. Number of ontries in  $K_S^0 \pi^+$  vs.  $K_S^0 \pi^-$  scatter plot in the  $K_S^0 \pi^-$  mass intervals 0.6650 - 0.8000 GeV, 0.8225 - 0.9575 GeV, and 0.9800 - 1.1150 GeV.

## Figure Captions

Fig.1: a) Missing mass squared for all  $K_S^0 K_S^0 \pi^+ \pi^- \pi^-$  final state events. The shaded histogram corresponds to missing mass squared for all  $K_S^0 K_S^0 \pi^+ \pi^+ \pi^-$  final state events used as an estimate of non-diffractive background. The curve is an estimate of non-diffractive background obtained from the shaded histogram.

b) Missing mass squared for all  $K_S^0 K_S^0 \pi^+ \pi^- \pi^-$  final state events after the background curve in Fig. 1(a) has been subtracted.

c) Missing mass squared for the  $K_S^0 K_S^0 \pi^- \pi^-$  subsystem for  $K_S^0 K_S^0 \pi^+ \pi^- \pi^-$  events with missing mass squared less than  $16 \text{ GeV}^2$ . These events are an estimate of the background from  $K_S^0 K_S^0 \pi^+ \pi^- \pi^- \pi^0$ .

d) Missing mass squared for all  $K_S^0 K_S^0 \pi^+ \pi^- \pi^-$  final state events after the shaded histogram of Fig. 1(c) has been normalized to Fig. 1(b) and subtracted. This is our estimate of the diffractive component with all backgrounds subtracted.

Fig.2: The distribution of  $t'$  to the  $K_S^0 K_S^0 \pi^+ \pi^- \pi^-$  final state for events with  $MM^2 < 16 \text{ GeV}^2$ . The fitted curve is explained in the text.

Fig.3: a) The  $K_S^0 K_S^0$  effective mass distribution for events with  $MM^2 < 16 \text{ GeV}^2$ ,

b) the  $K_S^0 K_S^0$  effective mass distribution with  $X_F < 0.25$  for events with  $MM^2 < 16 \text{ GeV}^2$ ,

c) the  $K_S^0 K_S^0$  effective mass distribution with  $X_F > 0.5$  for events with  $MM^2 < 16 \text{ GeV}^2$ .

Fig.4: a) The  $K_S^0 \pi^-$  effective mass distribution for events with  $MM^2 < 16 \text{ GeV}^2$ ,

b) The  $K_S^0 \pi^+$  effective mass distribution for events with  $MM^2 < 16 \text{ GeV}^2$ .

Fig.5:  $M(K_S^0 \pi^+)$  vs.  $M(K_S^0 \pi^-)$  scatter plot for events with  $MM^2 < 16 \text{ GeV}^2$ .

Fig.6: a)  $K_S^0 K_S^0 \pi^+ \pi^-$  effective mass distribution for events in the central region of Table I (84 entries).

b)  $K_S^0 K_S^0 \pi^+ \pi^-$  effective mass distribution for events in the non-diagonal  $K^{*+-} K_S^0 \pi^{-+}$  regions of Table I (184 entries).

c)  $K_S^0 K_S^0 \pi^+ \pi^-$  effective mass distribution for events in the corner (background) regions of Table I (127 entries).

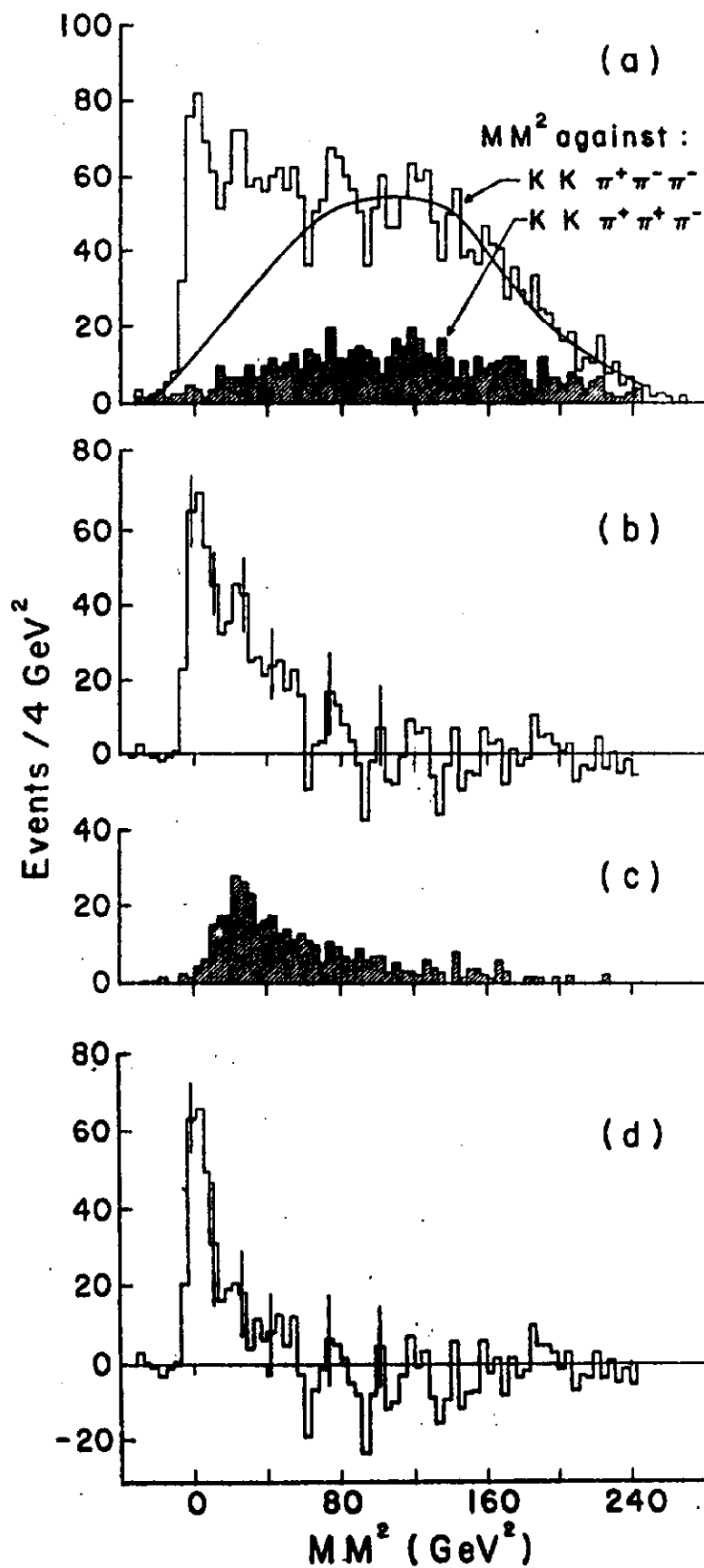
Fig.7: a) Background subtracted  $K^{*+} (890) K^{*-} (890)$  effective mass distribution (net of 35 entries).

b) Background subtracted  $K^{*+-} (890) K_S^0 \pi^{-+}$  effective mass distribution (net of 92 entries).

Fig.8:  $K_S^0 K_S^0 \pi^+ \pi^- \pi^-$  effective mass distribution for events with  $MM^2 < 16 \text{ GeV}^2$ . The shaded histogram corresponds to each entry in the central region of Table I.

Fig.9: Background subtracted  $K^{*+-} (K_S^0 \pi^{-+} \text{ inclusive})$  effective mass distribution for events with  $MM^2 < 16 \text{ GeV}^2$ .

Figure 1



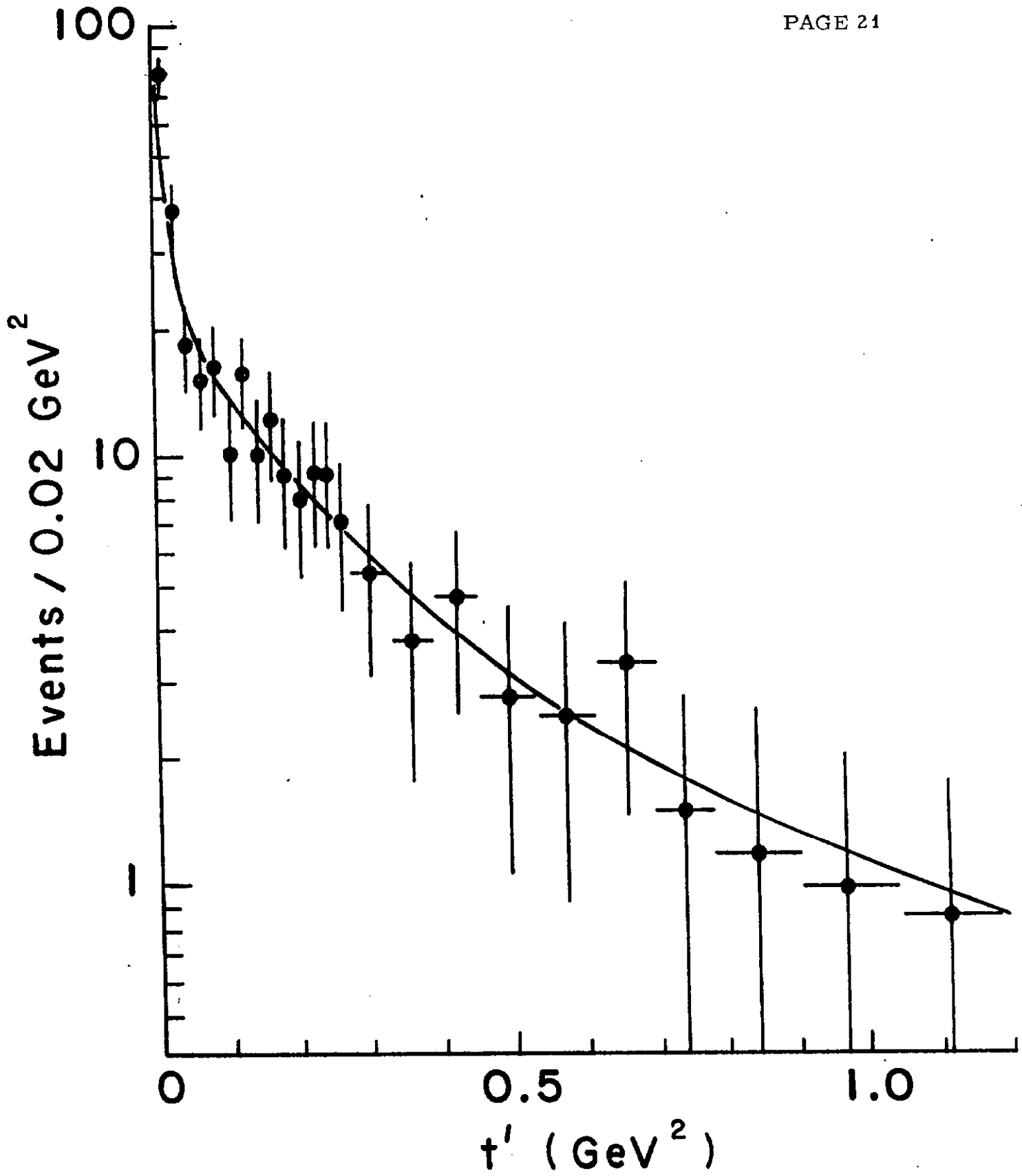


Figure 2

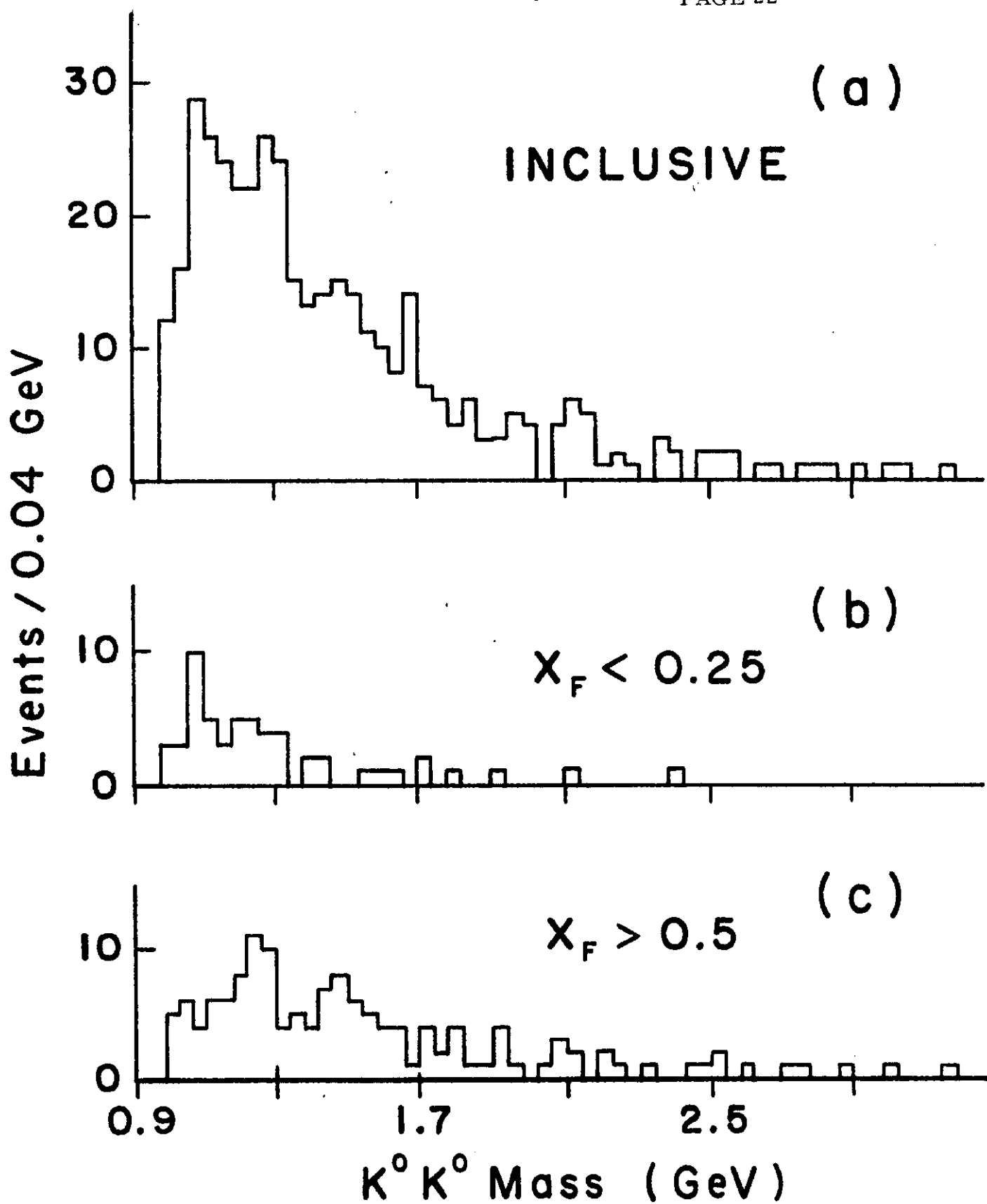


Figure 3

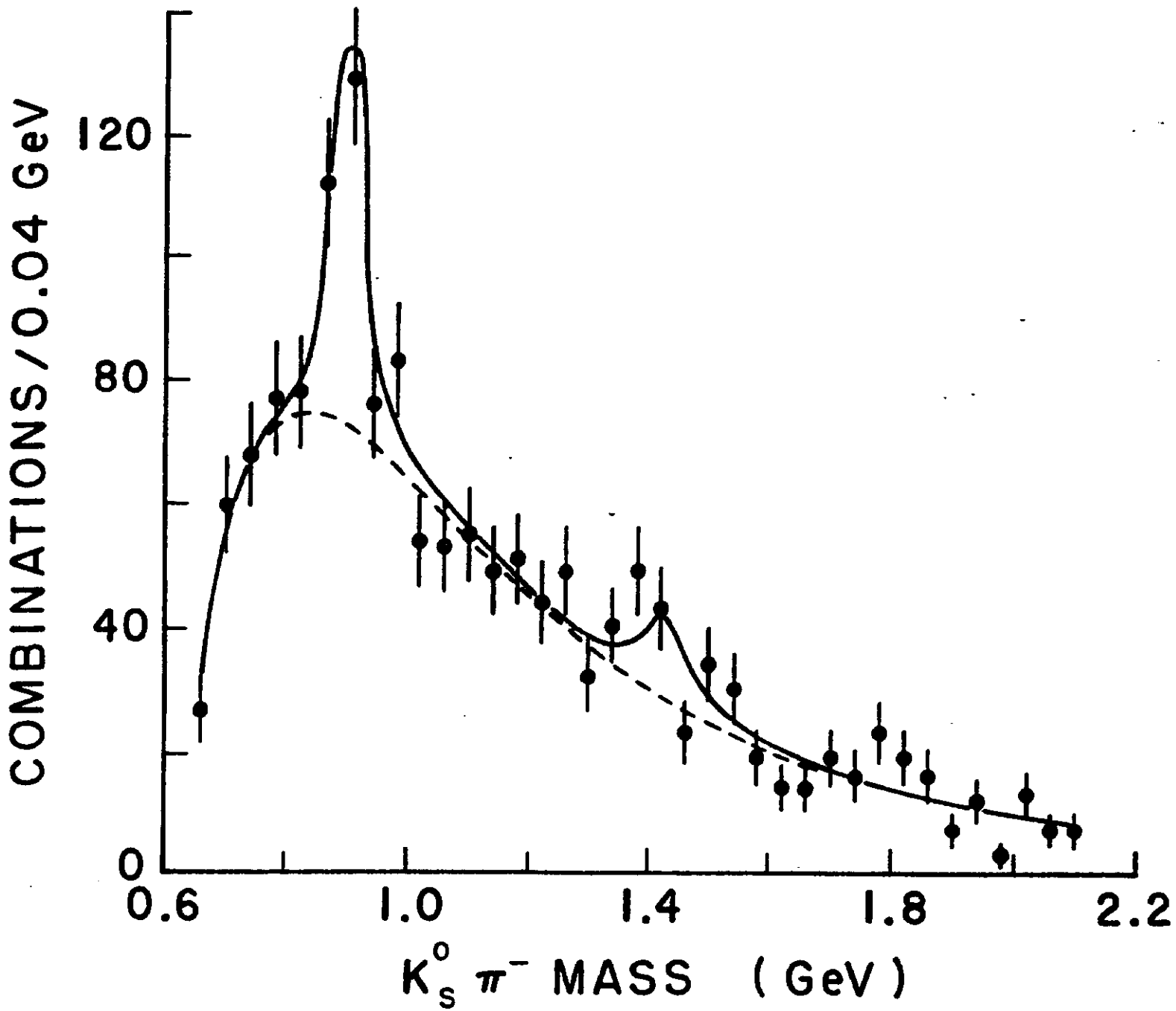


Figure 4(a)

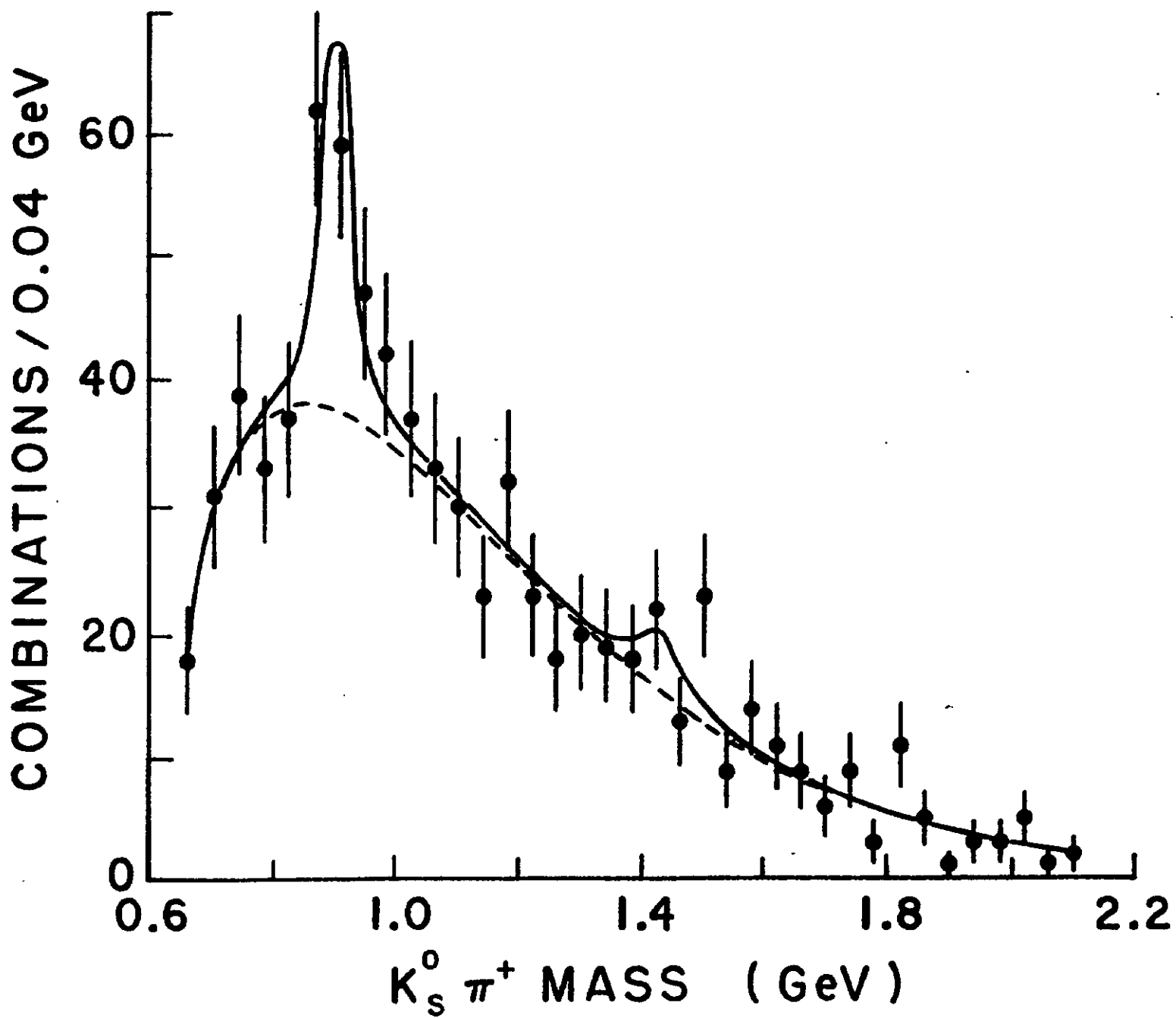


Figure 4(b)

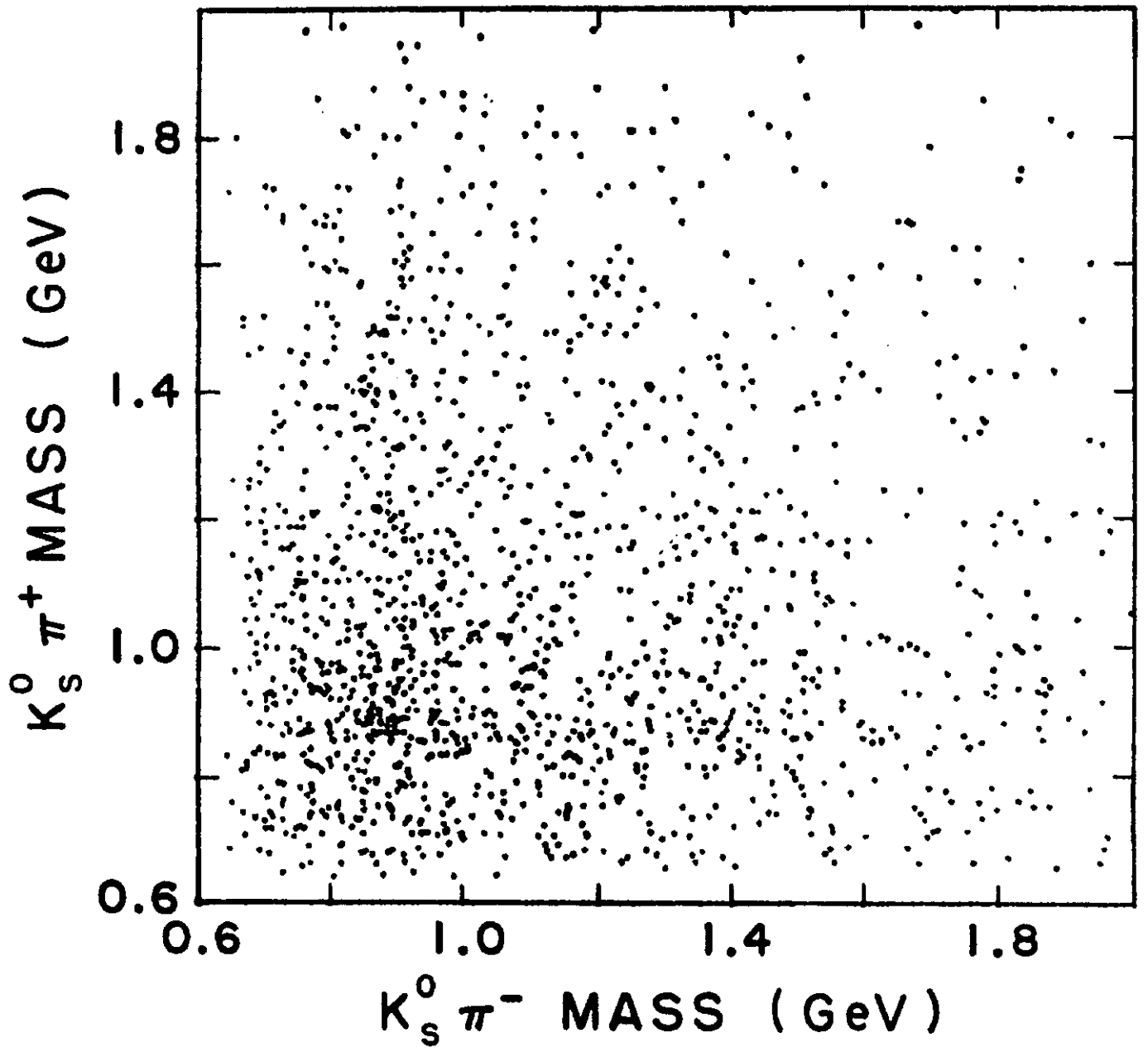


Figure 5

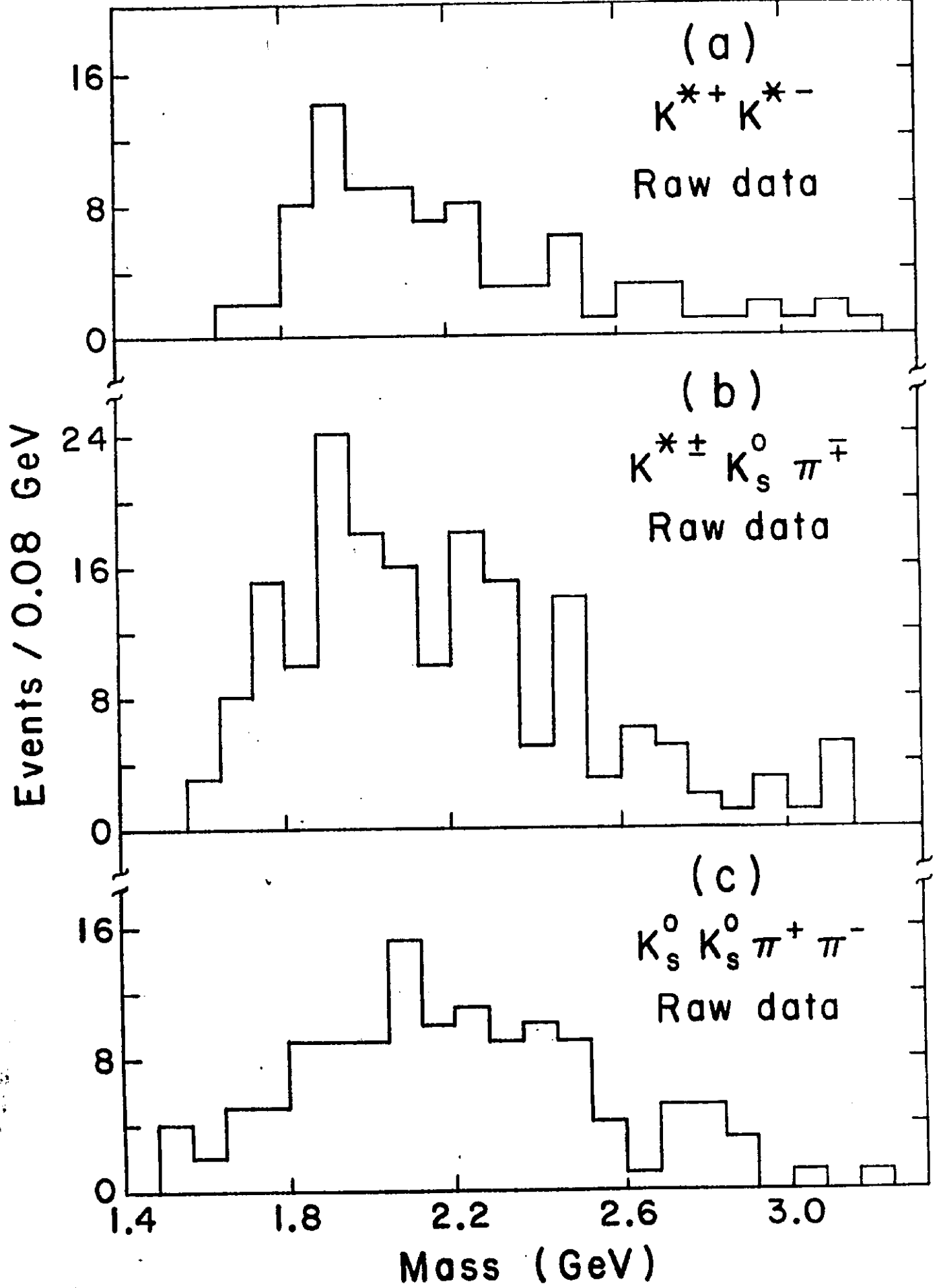
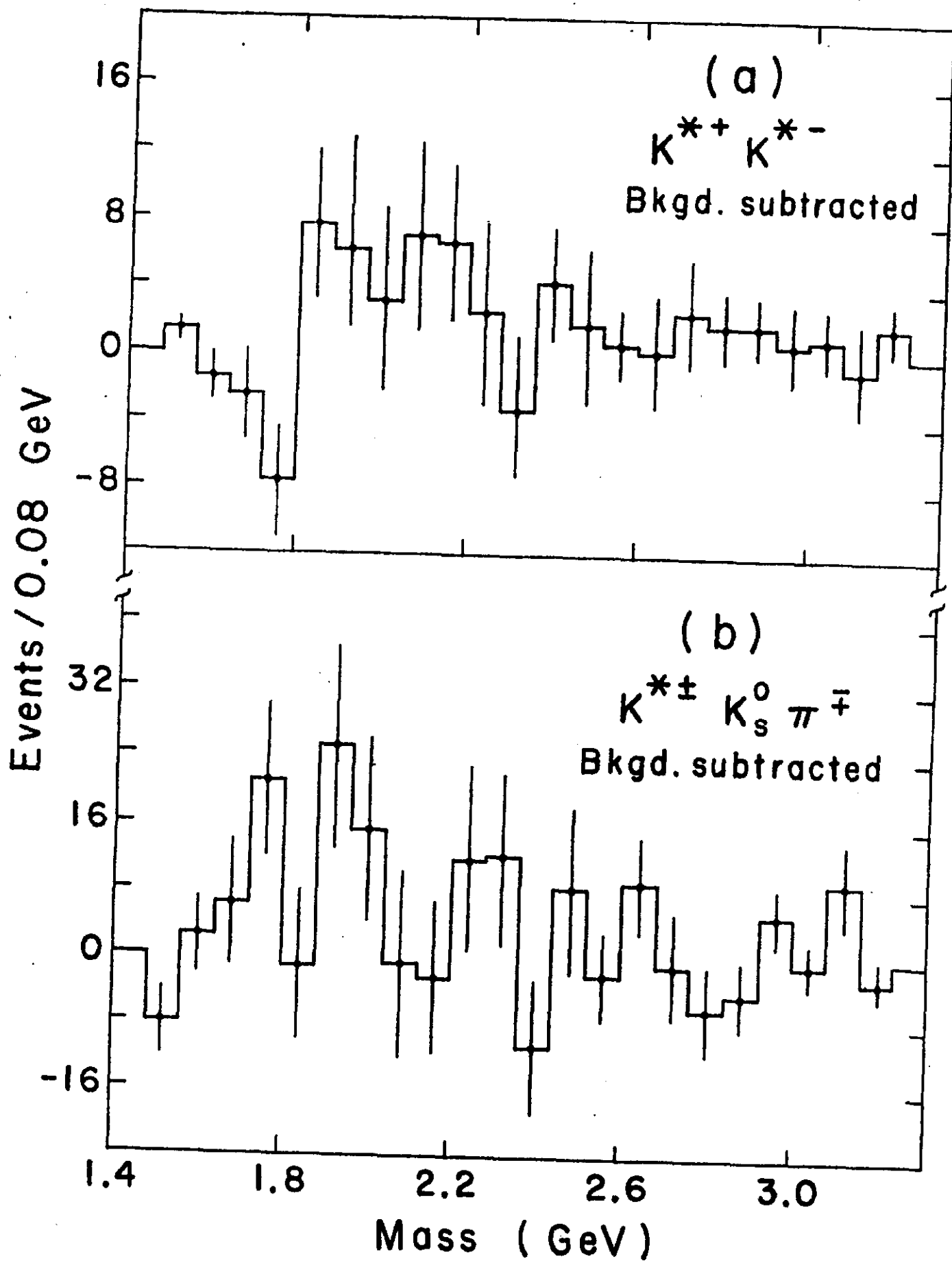


Figure 6



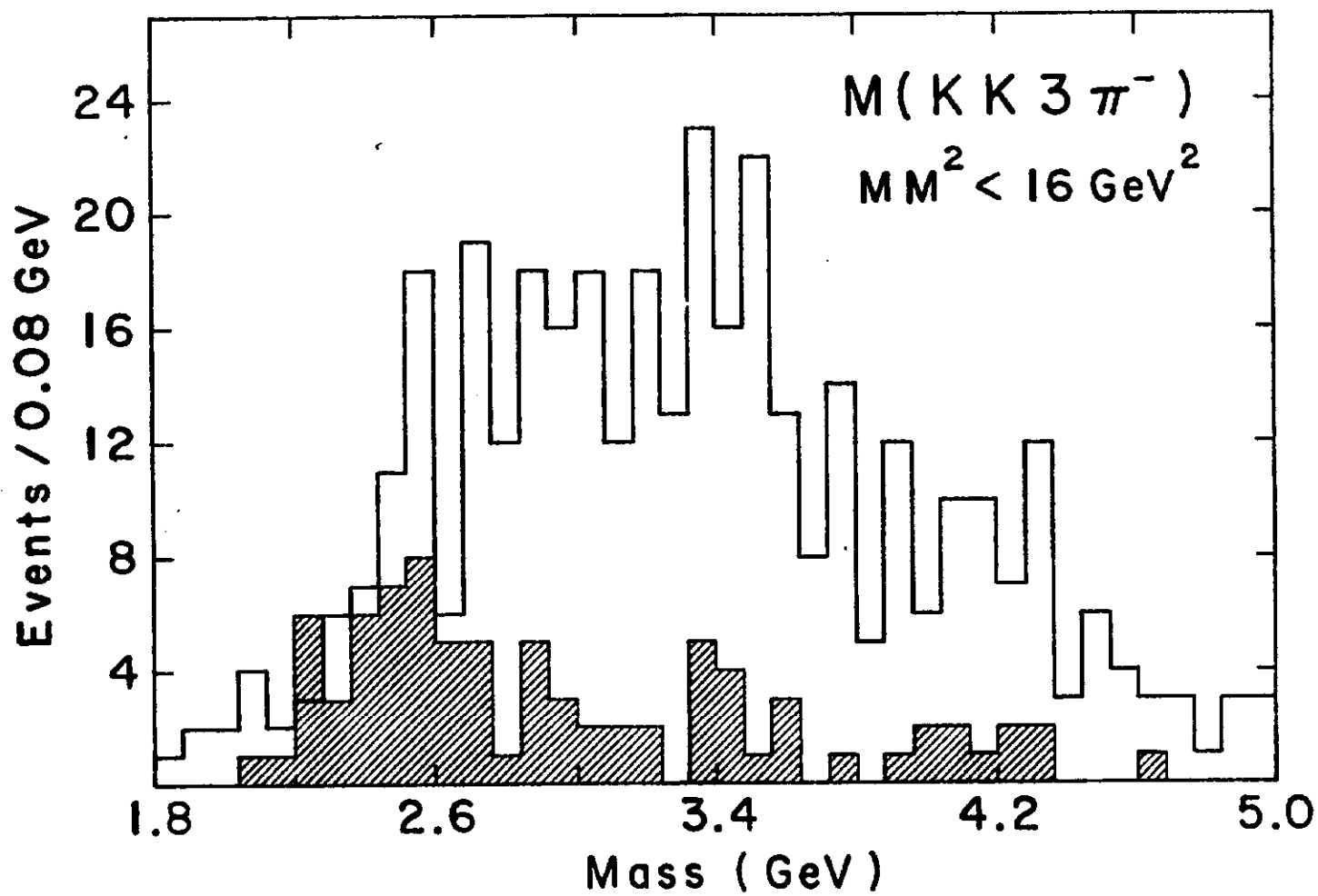


Figure 8

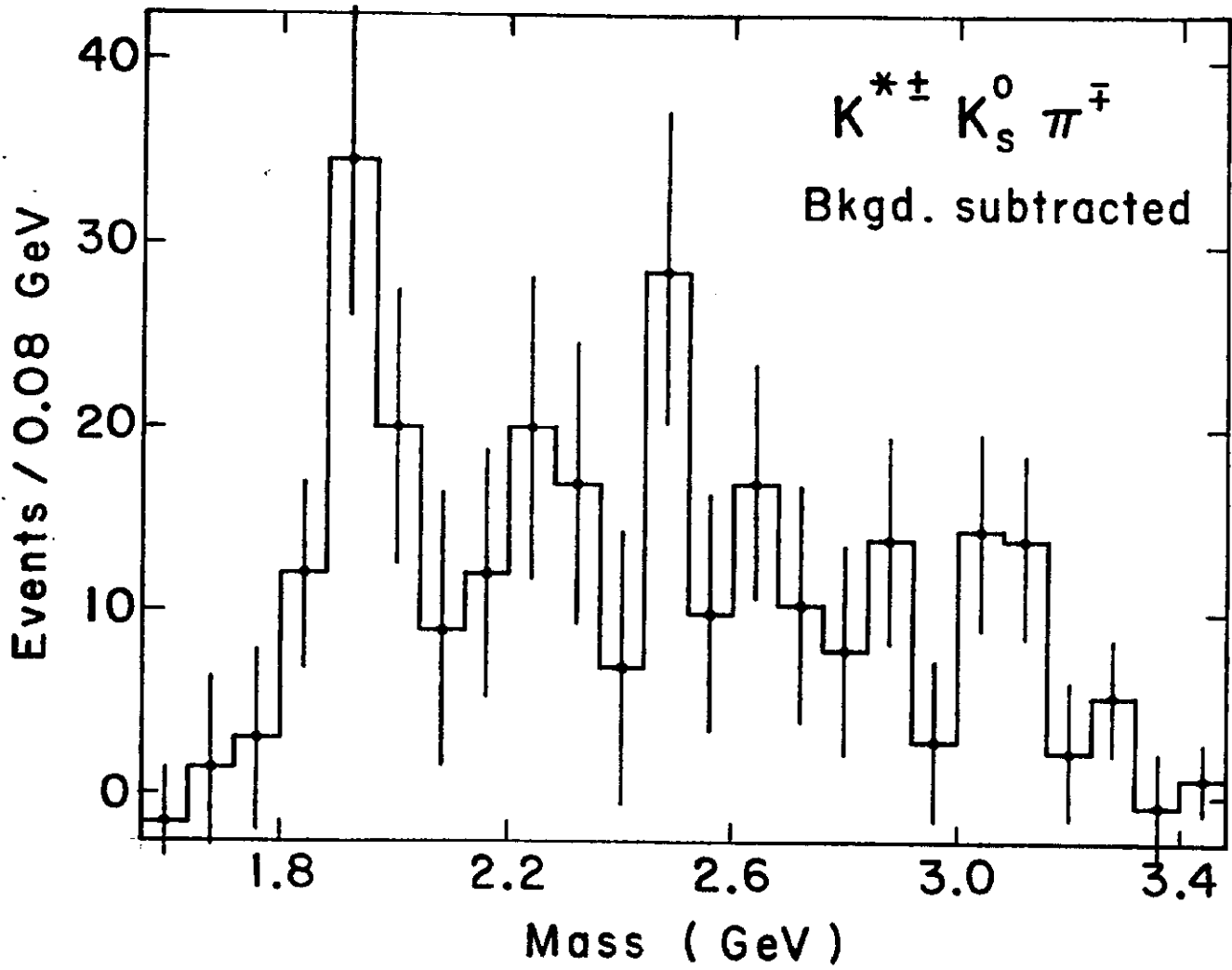


Figure 9